Journal of Molecular Graphics and Modelling 119 (2023) 108382

Contents lists available at ScienceDirect

Journal of Molecular Graphics and Modelling

journal homepage: www.elsevier.com/locate/jmgm

Piperidine-based natural products targeting Type IV pili antivirulence: A computational approach

Aslihan Ozcan [a], Ozlem Keskin [b], Berna Sariyar Akbulut [a], Pemra Ozbek [a,*]

[a] Faculty of Engineering, Department of Bioengineering, Marmara University, Istanbul, Turkey
[b] College of Engineering, Chemical and Biological Engineering, Koc University, Istanbul, Turkey

ARTICLE INFO

Keywords:
Antivirulence
Drug discovery
Molecular docking
Molecular dynamics simulations
Natural product
PilB
PilF
Piperidine
Type IV pili
Virtual library screening

ABSTRACT

Type IV (T4) pilus is among the virulence factors with a key role in serious bacterial diseases. Specifically, in *Neisseria meningitidis* and *Pseudomonas aeruginosa*, it determines pathogenicity and causes infection. Here, a computational approach has been pursued to find piperidine-based inhibitor molecules against the elongation ATPase of T4 pili in these two selected pathogens. Using the modeled structures of the PilF and PilB ATPases of *N. meningitidis* and *P. aeruginosa*, virtual library screening via molecular docking has returned inhibitor molecule candidates. The dynamics of the best three binders have further been investigated in detail via molecular dynamic simulations. Among these, ligands with COCONUT IDs CNP0030078 and CNP0051517 were found to have higher potential in the inhibition of ATPases based on molecular dynamic simulation analysis and biological activity information. The obtained results will guide future efforts in antivirulence drug development against T4 pili of *N. meningitidis* and *P. aeruginosa*.

1. Introduction

Irresponsive use of available antibacterial drugs leading to the development of resistance mechanisms and an increase in the number of multidrug-resistant strains makes it extremely difficult to timely manage the spread of infectious disease [1]. In this context, molecules that target bacterial virulence become an alternative to traditional antimicrobials. Instead of killing the pathogens that cause infections, antivirulence therapies cleanse the pathogens from their weapons [2,3]. Targeting antivirulence is an attractive approach, however lack of firm evidence on antivirulence targets and their mechanistic details, make antivirulence a field that requires intensive research.

Type IV (T4) pilus, also known as the "Swiss Army knife", is a virulence factor with key roles in various bacterial diseases. It is utilized for twitching motility, biofilm formation, cell-cell interactions, surface adhesion, and competence across different species. Biogenesis machinery of a T4 pilus is made up of multiple sub-complexes, each of which is necessary for the system to function [4]. ATPases, platform proteins, and pilins are the most easily recognized and highly conserved components in T4 pili. In a typical pilus, pilin proteins are organized in a helical array, with the core filled with conserved hydrophobic amino-terminal-helices and the outside shell made up of more variable carboxy-terminal globular domains [5,6]. The cytoplasmic hexameric elongation and retraction ATPases, are required to generate the motor forces for polymerization and depolymerization, respectively [7]. In the current work, inhibitor candidates are searched targeting the elongation ATPases, PilF of *N. meningitidis* and PilB of *P. aeruginosa* that energize the assembly of T4 pili.

N. meningitidis, generally known as meningococcus, is the primary cause of bacterial meningitis across the world [8]. It leads to a serious infectious disease that can result in death or disability in both children and adults [9]. Before passive immune or antibiotic therapies became available, invasive meningococcal illnesses had a fatality rate of 70% to 90%. If left untreated, this disease is deadly in 50% of the cases and 10-20% of the survivors may suffer from brain damage, hearing loss, or disability [10]. *N. meningitidis* is readily spread through saliva and the respiratory tract by coughing or sneezing. The polysaccharide capsule, which prevents phagocytosis and helps *N. meningitidis* to escape from the defense mechanism of the host cell [11], and the fimbriae, which allow bacteria to adhere to epithelial cells [12] are among its virulence factors. Recent studies have proposed T4 pili, which is required for bacterial aggregation, twitching motility, natural transformation, adhesion, and signal transduction with host cells [13], as a target for antivirulence therapies against meningococcal diseases caused by *N. meningitidis*

* Corresponding author.
E-mail address: pemra.ozbek@marmara.edu.tr (P. Ozbek).

https://doi.org/10.1016/j.jmgm.2022.108382
Received 19 August 2022; Received in revised form 1 November 2022; Accepted 23 November 2022
Available online 26 November 2022

[14–16]. On the other hand, *P. aeruginosa* is a pathogen that is commonly associated with hospital-acquired infections. Pseudomonas infections often result in death, especially in people with cystic fibrosis [17]. This bacteria is also the reason for about 5% of neonatal meningitis [18]. It poses a serious clinical problem due to its opportunistic nature [19]. Its biofilm-forming ability promotes surface attachment and this makes it difficult to completely eradicate *P. aeruginosa* infections [20]. The exopolysaccharides, lipopolysaccharides, proteases, lipases, elastases, and T4 pili are among the factors that make *P. aeruginosa* a highly flexible pathogen [21,22]. T4 pili aid in twitching motility and adhesion, thereby allowing colonization in *P. aeruginosa* [13]. Evidence shows that T4 pili have a proven role in the pathogenicity of both *N. meningitidis* and *P. aeruginosa*.

To date, there has been limited endeavor focusing on the T4 pili as an antivirulence target. Only a few of them used computational methods. The PilF ATPase has first been proposed to be a therapeutic druggable target by Aubey et al. [15]. In this study, druggable binding sites on PilF were predicted by computational molecular docking. Through experimental studies, they were able to identify three compounds that inhibited PilF of *N. meningitidis*, which in turn prevented microcolony formation on endothelial cell surfaces. Among these compounds, the most effective, 1-((piperidin-4-yl)methyl)piperidin-4-ol (P4MP4), was found to possess the following three moieties; 2,4-dimethoxybenzene, piperidine, and naphthalene. Activity of these compounds was attributed to the presence of piperidine and 2,4-dimethoxybenzene. At around the same time, Denis et al. [14] reported that trifluoperazine and related phenothiazines can block functions associated with T4 pili in *N. meningitidis*. Trifluoperazine is a family of phenothiazine derivatives that comprises three moieties: aliphatic compounds, piperidines, and piperazines. In a more recent high throughput screening study, Dye et al. [23] identified quercetin as an inhibitor of the T4 pili ATPase, PilB, of *Myxococcus xanthus*, which subsequently reduced T4 pili-dependent motility and T4 pilus assembly.

Motivated by the activities of molecules with piperidine moieties against the elongation ATPase of T4 pili [14,15], the current work employs a docking-based virtual screening and molecular dynamics (MD) approach to identify inhibitors with piperidine moieties to intervene the interaction of T4 pili with the surfaces they infect. Here, two natural products (COCONUT IDs CNP0030078 and CNP0051517) have been identified as potential inhibitors of the PilF and PilB subunits of T4 pili in *N. meningitidis* and *P. aeruginosa*, respectively. These ligands were also predicted to possess biological activity against nervous system-related diseases.

2. Methods

2.1. Homology modelling and binding site prediction

The 3-dimensional (3D) structure models of the proteins were constructed with Swiss-Model [24] server using sequence information provided in UNIPROT [25].

UniProtKB IDs of T4 pilus assembly protein PilF of *N. meningitidis* serogroup B (strain MC58) and of PilB of *P. aeruginosa* (strain ATCC 15692/DSM 22644/CIP 104116/JCM 14847/LMG 12228/1C/PRS 101/PAO1) are Q7DDR2 and P22608, respectively. T4 pilus biogenesis ATPase PilB of *Geobacter sulfurreducens* (strain ATCC 51573/DSM 12127/PCA) structure [PDB ID: 5ZFR; crystal structure of PilB, an extension ATPase motor of Type IV pilus from *Geobacter sulfurreducens*, 3.10 Å] [26] with the UniProtKB ID of Q74D28 was used as a template for modelling the ATPase structures. Obtained models were analyzed using the Saves v6.0 server (https://saves.mbi.ucla.edu/).

The binding sites of the constructed PilF and PilB models were predicted using MetaPocket 2.0 [27]. The ATP/ADP binding pockets of the enzymes were also retrieved from LIGPLOT [28] using the ADP bound PilB structure of *G. metallireducens* (PDB ID: 5TSG) [29]. The potential binding sites determined in a recent study [15] and the ATP/ADP binding region of the related T4 pilus proteins coincide with MetaPocket 2.0 results. Hence, the relevant binding sites were selected accordingly.

2.2. Library selection, database filtering

The online version of the COlleCtion of Open Natural prodUcTs (COCONUT) resource [30] was used for accessing natural drugs with a piperidine moiety. This is a dataset aggregated from elucidated and predicted natural products and it has been used in recent virtual library screening studies that focus on natural products [31–35]. As of December 2021, 4999 natural products with piperidine were downloaded in a single file and filtered using FAF-Drugs4 (Free ADME-Tox Filtering Tool) [36]. Drug-Like Soft filter, the Pan Assay Interference Compounds (PAINS) filter, and Lipinski Rule of five were selected to refine drug selection. PAINS moieties, which stands for Pan Assay Interference Compounds, are molecules that emerge as frequent hits (promiscuous compounds) in several biochemical high throughput screens, according to Baell et al. [37]. The Drug-Like Soft filter is created by FAF-Drugs4 by integrating many publications [38–40] discussing the physico-chemical features of drugs with an in-house statistical analysis of pharmaceuticals. In the Lipinski Rule of five filter; a molecule with a molecular mass of less than 500 Da, no more than 5 hydrogen bond donors, no more than 10 hydrogen bond acceptors, and an octanol-water partition coefficient log P not greater than 5 was considered more water-soluble and has high gastrointestinal absorption [41].

2.3. Molecular docking based virtual screening

The modeled structures of PilB and PilF ATPases were used as the targets for molecular docking. To prepare the target proteins and the ligands, water molecules were removed, missing hydrogens were added. Gasteiger charges were also computed in this step.

Virtual screening was conducted via AutoDock Vina [42] plugin of the open-source software PyRx [43] with the default parameter values. The search space was created as a box with dimensions of 27 Å × 27 Å x 27 Å to include all active site residues. Ligand bonds were allowed to rotate freely, while the receptor was kept rigid. To obtain the best binders and the binding modes, the selected library was screened five times for both targets.

To evaluate docking results, the ligands with the lowest binding energies were selected, and then MD simulations were conducted to test the ligands' stability in the binding groove. Furthermore, interaction bonds formed between the target protein and the ligands were analyzed using Discovery Studio Visualizer 2020 [44].

2.4. MD simulations for protein-ligand complexes

The stabilities of the docked ligands in the binding pocket of the proteins were evaluated via two parallel 100 ns MD simulations of the selected protein-ligand complexes. NAMD (version 2.15 ALPHA) [45] and CHARMM36 force field [46] were used for all simulations. Ligand parameters were obtained from CHARMM-GUI modules (http://www.charmm-gui.org/input/ligandrm) [47]. TIP3P water molecules were used to solvate the target protein in a box with at least 12 Å padding distances to the periodic box boundary in each axis. The net charge of the system was neutralized by replacing randomly selected water molecules with an adequate amount of sodium and chloride ions. To relax probable steric clashes in the system, all systems were treated to 5000 steps of gradient-descent energy minimization. After minimization, 100 ns long equilibration/production MD simulations were performed. The Langevin thermostat and barostat were used to keep the temperature and pressure at 310 K and 1 bar, respectively. The minimum distance between the atoms of the interacting residues of each protein and ligand was computed to analyze the interactions of the selected molecules with PilB and PilF. Root mean square deviation (RMSD) was used to characterize ligand mobility during simulations. H-bonds were compared

between all protein-ligand complex systems to explain various dynamic processes attributable to H-bond occupancy. Additionally, the MD simulation trajectories were utilized in the Molecular Mechanics/Poisson-Boltzmann Surface Area (MM/PBSA) approach to calculate the energy of protein and ligand binding. To this end, a VMD plugin, the Calculation of Free Energy (CaFE) tool [48] was used. DelPhi [49] was applied to solve the Poisson-Boltzmann calculation model. For the MM/PBSA calculations, 50 frames from the last 20 ns of MD simulation trajectories were selected for all the complex simulations. The internal and external dielectric constants were taken as default values, 1.0 and 80.0, respectively, and the grating spacing reciprocal was set to 1.0 Å. The average binding free energy for each complex was obtained for the selected frames.

As a final step, PASS software [50] was used to evaluate the effectiveness potential of the candidate drug molecules. This server provides biological activity predictions based on the structure of a drug-like compound and gives Pa and Pi values as an output. The Pa value is an estimation of the probability to be active and should be higher than 0.5, while the Pi value is an estimation of the probability to be inactive and should be less than 0.1 for significant activity [50]. Here using this server, compounds' biological activity profiles were predicted and compared with the diseases associated by *P. aeruginosa* and *N. meningitidis*.

3. Results

3.1. Homology modelling

PilB has a total of 566 amino acid residues, while PilF has a total of 558 amino acid residues with 536 of them being homologous in the two sequences. For homology modelling of the ATPases, Swiss-Model was used with the same template for both enzymes based on their high similarity.

We have checked the quality of our models using Ramachandran plot, VERIFY 3D and ERRAT modules. The results are displayed in Figs. S1–S2 and Table 1 summarizes the performance results obtained from the quality tests.

3.2. Target site determination

For each ATPase, three potentials partially overlapping ligand binding sites have been predicted by MetaPocket 2.0. Details of the predicted pockets are given in the supporting file (Fig. S3). To a large extent, these sites coincided with the ATP/ADP binding sites of the enzymes, which were determined with LigPlot based on the ADP bound structure of PilB from *G. metallireducens* (PDB ID 5TSG). The ATP/ADP binding site residues are displayed in Fig. 1. Then a binding site for docking has been selected that encompassed the predicted three pockets and the ATP/ADP binding region and this site was used for further virtual screening.

3.3. Filtration of the ligand database

Natural products for screening were retrieved from the COCONUT database. Among the 4999 natural products with a piperidine moiety in COCONUT, 528 duplicates, 1 large molecule, and 2 molecules with isotope and inorganic groups were eliminated using FAF-Drugs4. Then Drug-Like Soft, PAINS and Lipinski Rule of 5 filters (Table S2) were applied to get 3118 molecules for virtual screening.

Table 1
Quality test results of homology models.

	Ramachandran plot	VERIFY 3D	ERRAT module
PilB	93.20%	98.18%	97.18
PilF	93.50%	91.99%	98.35

3.4. Molecular docking

After filtration of the database, the remaining 3118 molecules were docked 5 times onto the modeled ATPase structures and for each ligand, the average of binding energies obtained from 5 independent runs were used for further evaluation. First, molecules with binding energies lower than −9.0 kcal/mol for both PilF and PilB structures were filtered. The 26 ligand molecules common for PilF and PilB are listed in Table 2, along with their averaged binding energies. Then the top three binders (CNP0051517, CNP0030078, and CNP0196659) were selected for further analysis. Since the first poses of the 5 docking repetitions overlapped, one of them was arbitrarily chosen for each ligand and further study was carried out on this model (Fig. S4). Using Discovery Studio Visualizer, critical interactions between the ligands and the receptor-binding sites that include H-bonding, halogen bonding, and hydrophobic contacts were identified analyzing the 2D and 3D interactions of the docking results of these three ligands.

CNP0051517, 11-benzoyl-5-[3-(trifluoromethyl)phenyl]-7,11-diazatricyclo[7.3.1.$0^{2,7}$]trideca-2,4-dien-6-one, was docked to PilF forming H-bonds with Gln441 and Tyr500. Five amino acids (Leu290, Val323, Ile348, Leu443, Arg496) of PilF were involved in hydrophobic interactions with CNP0051517, as shown in Fig. 2(a). Among these, Leu290, Val323, and Leu443 are in the ADP/ATP binding site. When the same ligand was docked to PilB, similar interactions were found. Gln452 and Tyr508 formed H-bonds, while there were hydrophobic interactions with Leu301, Val334, Ile359, Leu454, Arg504 and the side chains of the ligand (Fig. 2(b)). Among these, Leu301, Val334, and Leu454 reside in the ADP/ATP binding site.

CNP0030078, 11-(4-fluorobenzoyl)-5-[3-(trifluoromethyl)phenyl]-7,11-diazatricyclo[7.3.1.$0^{2,7}$]trideca-2,4-dien-6-one, was docked to PilF forming H-bonds with Val323 and Tyr500 (Fig. 3(a)). There were hydrophobic interactions between Ala283, Leu290, Val323, Ile348, Leu443, Arg496 of PilF and the side chains of CNP0030078. It also formed a halogen bond with Thr322 of PilF. Among the H-bonding residues, Val323 resides in the ADP/ATP binding site. Leu290, Val323, and Leu443, displaying hydrophobic interactions, and Thr322 displaying a halogen bond interaction with the ligand, are also located in the ADP/ATP binding site. When the same ligand was docked to PilB, it was found to form H-bonds with Ile288, Gln452, and Tyr508. There were also hydrophobic interactions among Leu301, Val334, Ile359, Leu454, Arg504, Leu454, and the side chains of CNP0030078 (Fig. 3(b)). Among these sites; Leu301, Val334, and Leu454 are located in the ADP/ATP binding site.

CNP0196659, 1-benzyl 4-(4,7-dimethyl-2-oxo-2H-chromen-5-yl) piperidine-1,4-dicarboxylate was docked to PilF forming H-bonds with Ser284, Gln441, and Arg496. There were hydrophobic interactions between Leu290, Val323, Ile348, Leu443 and the side chains of the ligand (Fig. 4(a)). Among these, Leu290, Val323, and Leu443 residues are located in the ADP/ATP binding site. Similarly, the same ligand was also docked to PilB and formed H-bonds with Gln452, Arg504, and Tyr508. There were also hydrophobic interactions between Leu301, Val334, Ile359, Leu454 and the side chains of CNP0196659 (Fig. 4(b)). Residues Leu301, Val334, and Leu454, which formed hydrophobic bonds with CNP0196659, are located in the ADP/ATP binding site.

As a common feature, all these three ligands interacted with the three residues residing in the ATP/ADP binding site of PilF (Leu290, Val323 and Leu443) and PilB (Leu301, Val334 and Leu454). Furthermore, all three drug molecules formed hydrophobic interactions and bound to Leu290, Val323, and Leu443 in PilF and the corresponding residues Leu301, Val334, and Leu454 in PilB.

3.5. Analysis of MD simulations

MD simulations were performed on the ATPases with the docked ligands to evaluate the stability of the bound structures. RMSD profiles of the top three binder molecules are given in Fig. 5. The results

PilB (PDB ID: 5TSG)	PilB (*P. aeruginosa*)	PilF (*N. meningitidis*)
LEU300	LEU301	LEU290
GLY328	GLY329	GLY318
SER329	SER330	SER319
GLY330	GLY331	GLY320
LYS331	LYS332	LYS321
THR332	THR333	THR322
VAL333	VAL334	VAL323
LEU453	LEU454	LEU443

Fig. 1. ADP binding residues (gray balls) of PilB (PDB ID 5TSG) (shown in green) and their analogous residues in PilB (depicted in red) and PilF (depicted in blue) modeled structures. (For interpretation of the references to colour in this figure legend, the reader is referred to the Web version of this article.)

Table 2
Average binding affinities (kcal/mol) obtained from molecular docking.

COCONUT ID	MOLECULAR FORMULA	BINDING AFFINITY VALUES (kcal/mol)	
		PILB	PILF
CNP0051517	C25H21F3N2O2	−9.58 ± 0.39	−10.18 ± 0.04
CNP0030078	C25H20F4N2O2	−9.64 ± 0.19	−9.96 ± 0.05
CNP0196659	C25H25NO6	−9.40 ± 0.09	−9.66 ± 0.05
CNP0298576	[C26H26NO6]-	−9.48 ± 0.08	−9.52 ± 0.10
CNP0286303	C23H21NO8	−9.40 ± 0.19	−9.46 ± 0.08
CNP0065844	C25H21F3N2O3	−9.44 ± 0.05	−9.42 ± 0.07
CNP0043312	C25H20F4N2O3	−9.48 ± 0.04	−9.26 ± 0.08
CNP0065396	C24H21ClN2O2	−9.08 ± 0.08	−9.60 ± 0.00
CNP0061061	[C23H20NO6]-	−9.26 ± 0.11	−9.42 ± 0.04
CNP0310895	C25H25NO6	−9.16 ± 0.25	−9.50 ± 0.00
CNP0063223	[C26H26NO6]-	−9.32 ± 0.04	−9.32 ± 0.12
CNP0051132	[C28H37N4O3]+	−9.14 ± 0.00	−9.36 ± 0.05
CNP0224821	C25H25NO6	−9.48 ± 0.04	−9.00 ± 0.09
CNP0233509	C25H25NO6	−9.14 ± 0.05	−9.34 ± 0.05
CNP0383238	C26H27NO6	−9.44 ± 0.05	−9.00 ± 0.13
CNP0007146	C25H26FN3O2S	−9.20 ± 0.10	−9.22 ± 0.04
CNP0016525	C23H23N3O5	−932 ± 0.08	−9.02 ± 0.10
CNP0271224	C25H27N3O2S	−9.20 ± 0.12	−9.12 ± 0.10
CNP0280245	C24H23NO6	−9.10 ± 0.10	−9.20 ± 0.13
CNP0399110	C25H26FN3O2S	−9.06 ± 0.17	−9.22 ± 0.16
CNP0243153	C21H21 N	−9.08 ± 0.04	−9.18 ± 0.12
CNP0210462	[C25H28NO7]-	−9.24 ± 0.09	−9.02 ± 0.07
CNP0238559	C24H23NO6	−9.12 ± 0.16	−9.12 ± 0.12
CNP0040821	C24H21FN2O2	−9.16 ± 0.17	−9.00 ± 0.13
CNP0065750	C25H31FN4O3	−9.00 ± 0.07	−9.14 ± 0.10
CNP0044290	C26H31F2N3O3	−9.00 ± 0.12	−9.06 ± 0.08

indicated that the ligands CNP0051517 and CNP0030078 displayed lower mobility when complexed with either of the ATPases and remained stable throughout the simulations (Fig. 5).

The minimum distances between the protein residues and the ligands were calculated throughout the simulations to measure the strength of the interactions between ligands and proteins. For a strong interaction, the distance value between the donor and the acceptor is expected to be less than 3.5 Å [51].

Obtained results have shown that all three ligands (CNP0051517, CNP0030078, CNP0196659) remained in close vicinity of the target protein throughout the simulations with average distances of 2.05 ± 0.14 Å, 2.04 ± 0.14 Å and 2.01 ± 0.13 Å for PilB and 2.04 ± 0.15 Å, 2.11 ± 0.14 Å and 1.93 ± 0.11 Å for PilF, respectively (Fig. 6). The distances during the 100 ns trajectories remained within 2.1 Å, indicating strong binding (Fig. 6). The final conformations of the structures reached at the end of 100 ns simulations have shown that all three ligands retained their interactions with a valine residue only (Val290 of PilF and Val334 of PilB). The conformations of the protein-ligand complexes at the end of 100 ns MD simulations are also given in the Supporting Fig. S5.

The H-bond occupancies were analyzed and the results showed that H-bonds were conserved throughout the trajectories (Fig. 7). Critical H-bonding residues of PilF and PilB with an occupancy rate higher than 5% (for 2 parallel runs) are further detailed in Table S1. Among the target sites; Val323 of PilF and Val334 of PilB are present in the H-bonding network. They had consistent occupancy values over 5% for all 3 ligands (for each parallel simulation). The results are displayed in Table 3.

The H-bond formed between CNP0196659 and Val334 of PilF displayed the highest average occupancy of 26.09%. This was followed by CNP0051517 with an average occupancy of 23.87% with the Val334 residue of PilB. Supporting Fig. S6 displays the distances between Val323 of PilF and Val334 of PilB and the ligand molecules. For all 3 ligands (average of 2 parallel runs), the measured distances between these valine residues remained between 2 and 3 Å.

Finally, as a result of the MM/PBSA calculations, the average binding free energy of each complex was obtained for 50 snapshots retrieved

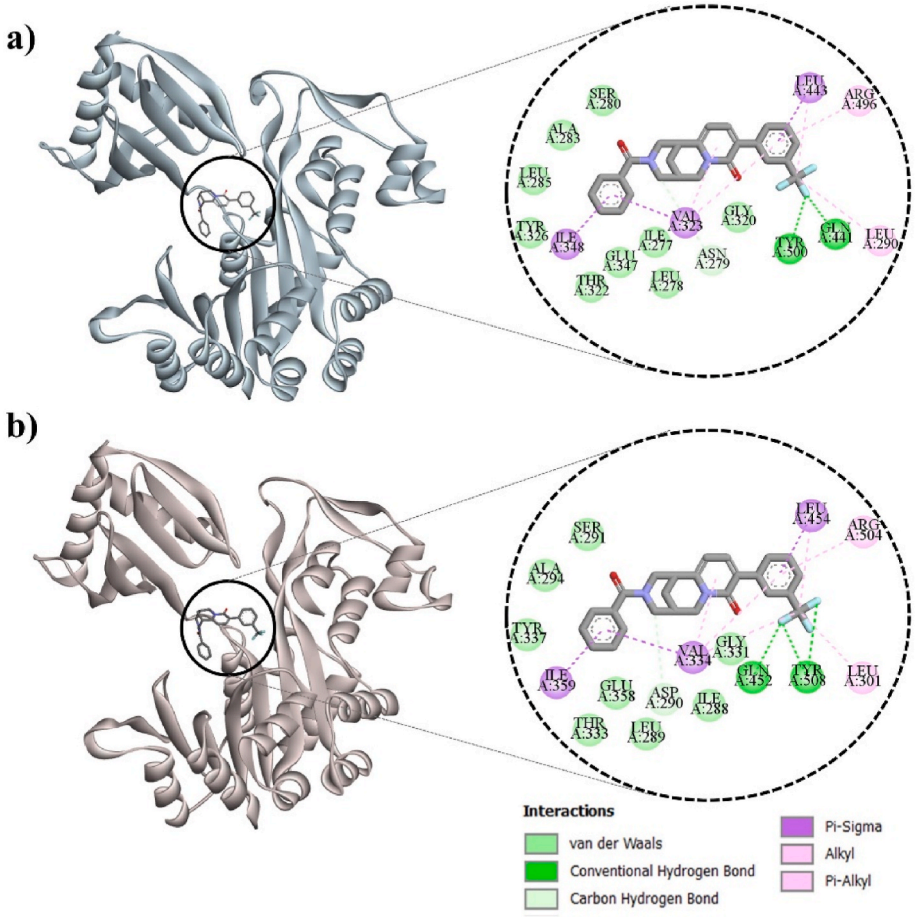

Fig. 2. Docked poses of CNP0051517 ligand and the 2D view of interaction profile of the ligand with the surrounding amino acids of (a) PilF and (b) PilB.

from the last 20 ns of the 100 ns trajectories (Table 4). CNP0051517 displayed the lowest binding free energy when bound to PilF, while CNP0030078 displayed the lowest binding free energy when bound to PilB. On the other hand, CNP00169659 displayed the weakest binding when bound to both PilF or PilB.

3.6. Evaluation of biological activities for potential drug molecules

The biological activities of the top three best binders were finally assessed using the PASS online server. The biological activities of the three ligands with significant Pa (higher than 0.5) and Pi (less than 0.1) values are given in Table 5.

Information obtained from the PASS server has shown that both CNP0051517 and CNP0030078 have activities against cognition disorders, mood disorders, sleep disorders, attention-deficit/hyperactivity disorder, antipsychotic, dependence, depression, anxiolytic, Parkinsonian, neurodegenerative diseases and Alzheimer's disease. On the other hand, CNP0196659 was predicted to be biologically active as a gastrin inhibitor, a spasmolytic urinary agent, a CYP2A11 substrate, a spasmolytic papaverin-like, and a phosphatase inhibitor.

4. Discussion

The virulence factor T4 pilus is a surface structure with key roles in adhesion to surfaces, twitching motility, modification of biofilm architecture, DNA uptake and exchange, secretion of exoproteins, and bacteriophage susceptibility [52]. Its ability to retract helps to bring the cell body into close proximity with a surface, allows migration along a surface away from the initial point of contact or toward an attractant, repositions cells in relation to one another (differentiation within a biofilm), and assists cells to efficiently escape from surfaces when necessary [53]. With all these activities, this multiprotein structure constitutes an important anti-virulence target. The T4 pili are energized by ATPases for pilus extension and retraction. Here the focus is on the inhibition of elongation ATPases, PilF and PilB, of the motor subcomplex of *N. meningitidis* and *P. aeruginosa*, respectively. We tried to seek for inhibitor molecules among natural products due to their diversity and wide range of bio-activities, which have made them attractive molecules for therapeutic purposes for more than 4000 years [54]. Here, particular emphasis was given to molecules with a piperidine scaffold. Piperidine is a significant building block in the production of many pharmacological molecules and is one of the most regularly utilized heterocycles among the US FDA-approved medications [55]. Many of its derivatives with a wide range of biological activities can also be extracted from plants.

In virtual screening and docking, accurate predictions depend on a good protein model and reliable information on the docking site. In this work, the 3D structures of the ATPases, PilF and PilB, under question were not available; therefore, modelling of these proteins was critically important in the design of inhibitors targeting them. In a previous study, Aubey et al. [15] has modeled the *N. meningitidis* PilF based on the crystal structure of *G. metallireducens* PilB (PDB ID 5TSG) using the HHpred server but their model was not available thus we have remodeled this ATPase using the same template. A successful homology model required 90% of the residues to reside in the desired area on the Ramachandran plot [56,57], while VERIFY3D should have a valid score (mean scores of residues should be greater than 0.2) [58] and the ERRAT quality value should be at least 90 [59]. Although the template structure had a relatively low resolution (3.10 Å), the quality of the modeled structure was found to be acceptable, based on evaluations with Ramachandran plot, VERIFY3D and ERRAT. Hence, the PilF and PilB

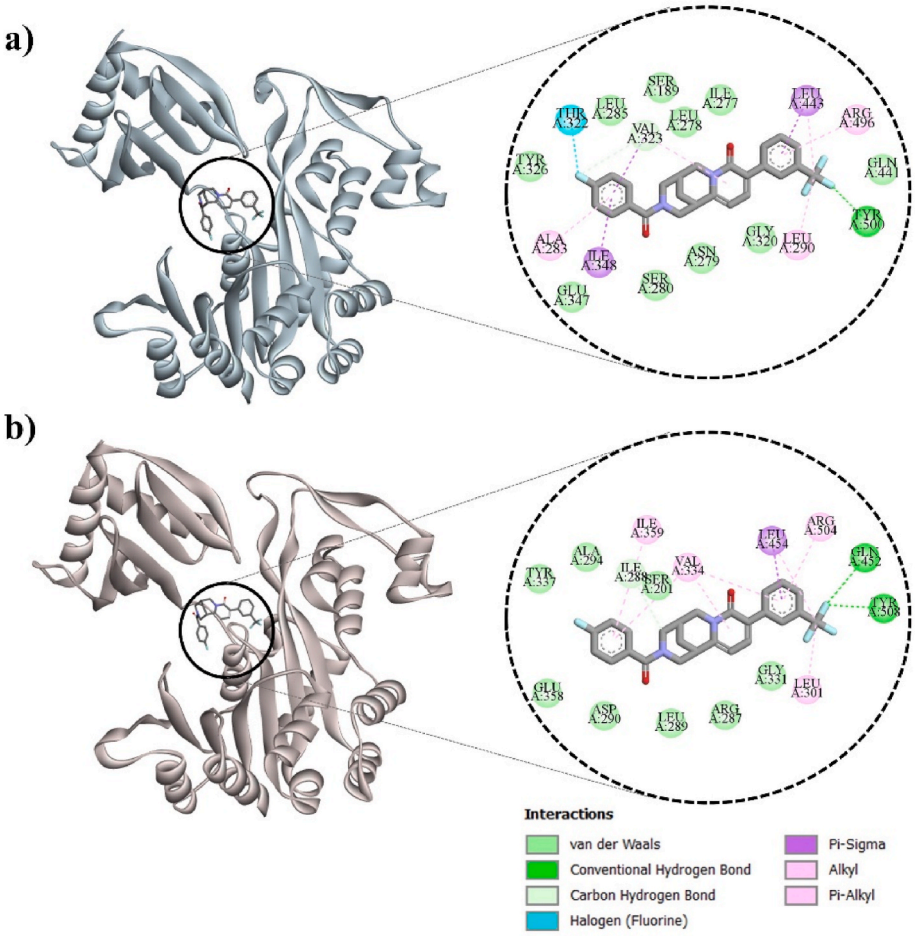

Fig. 3. Docked poses of CNP0030078 ligand and the 2D view of interaction profile of the ligand with the surrounding amino acids of (a) PilF and (b) PilB.

structures we have modeled by Swiss-Model were further used as target structures in virtual screening.

When the potential binding sites on the modeled PilB and PilF proteins were predicted, all results suggested the same region on the structure, which also coincided with the ATP/ADP binding pocket. Both proteins are ATPases meaning that ATP binds their active sites to be hydrolyzed to energize the pilus; hence, obstruction of this site with some other small molecule should be expected to directly impede its activity. Unfortunately, these is always a challenge when targeting the ATPases with these ATP-competitive inhibitors, since their ATP binding sites are highly conserved. However there is evidence that they do not necessarily inhibit other related ATPases [60,61]. Indeed, in a recently published study, the importance of ATP/ADP binding sites in ligand binding was underlined [62]. In their work, Dye and Yang investigated the binding of ligands to the separate domains and full-length form of *Myxococcus xanthus* PilB. They have demonstrated that the full-length PilB protein binds to ligands with greater affinity and that the presence of the ATPase domain improves ligand binding in the full-length PilB protein. They came to the conclusion that ADP binding residues, which were effective in ligand binding, also played an important role in inhibiting the T4 pili assembly ATPases and might therefore be used as inhibitor targets. In the earlier study by Aubey et al. [15], among the proposed residues important for inhibitor binding was Asp207 of *N. meningitidis* PilF, which resides in the close vicinity of the ATP/ADP binding region. This residue of PilF and the corresponding residue Asp219 of PilB were both predicted by MetaPocket 2.0 [27] to be in our binding site (Fig. S3). Different from our work, Aubey et al. [15] have used a hexameric ATPase model for predicting binding sites and therefore also proposed three additional residues, Arg457, Lys371, and Glu390, in the interface regions of the separate ATPases for inhibitor binding. All these findings indicate that the ATP/ADP binding region possesses great potential for inhibitor binding to modulate activity.

The obtained binding affinities (Table 2) have clearly shown that the potential inhibitor molecules strongly bind to our predicted ATP/ADP binding region. The valine and leucine involved in ATP/ADP binding were found to interact hydrophobically with the potential ligands and we believe they may deserve particular attention. In protein-ligand complexes, hydrophobic contacts through the side chains of leucine, valine, isoleucine, and alanine are known as the most prevalent type of interactions [63]. These side chains frequently form huge hydrophobic clusters that effectively prevent water from penetrating their underlying H-bond networks improving solvent exchange protection [64]. Chauhan et al. [65] have also demonstrated the importance of non-polar and hydrophobic amino acid residues such as valine and leucine for protein-ATP binding. When leucine was substituted with cysteine (Leu201Cys) in the retraction ATPase of *N. gonorrhoeae* in T4 pilus, hexamer formation was not affected while ATP hydrolysis rate was reduced by 50% [66]. Our results together with these reports underline the importance of leucine and valine in the binding pocket.

It is also possible to detect critical residues that interact with ligands in the target structure by analyzing the MD simulation results. The analysis of H-bond occupations in MD simulations helps to explain the stability of ligand molecules and predict critical residues of the targeted protein. Taking $\geq$ 5% as the critical value for H-bond occupancy [67], the simulations were interpreted. It was seen that all three top binders stably bind to their targets and form H-bonds. Among the residues selected for their high occupancy values, only Val323 of PilF and Val334 of PilB persistently gave values above the reference for all 3 ligands.

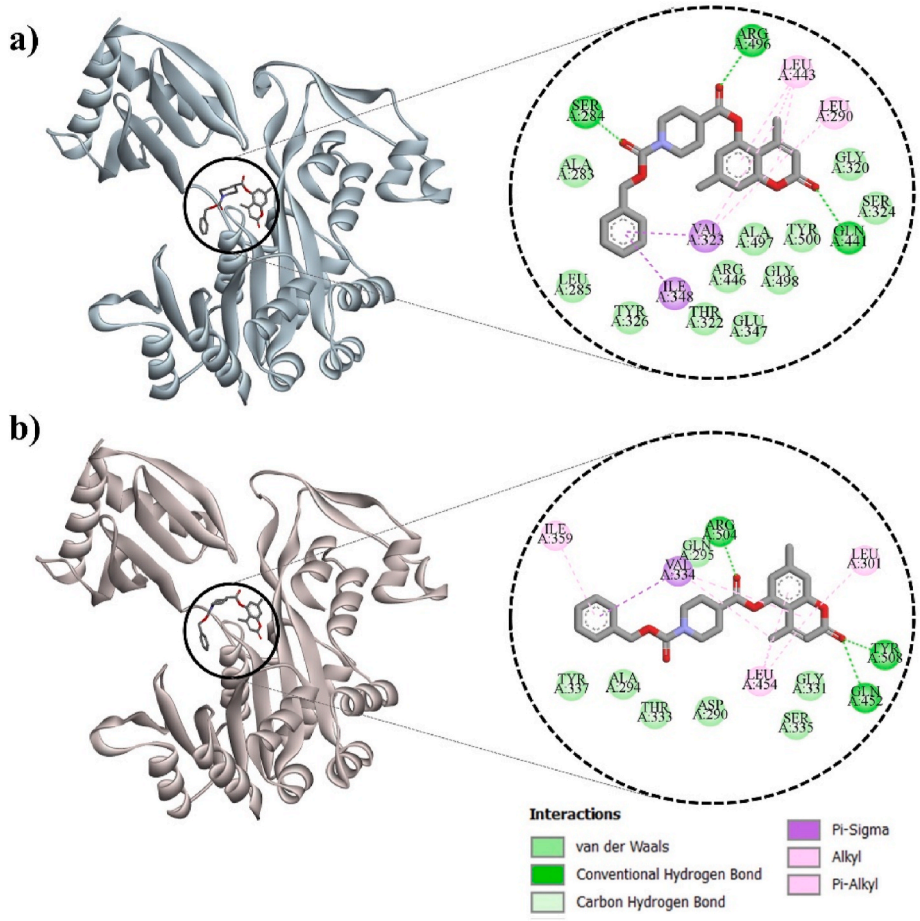

Fig. 4. Docked poses of CNP0196659 ligand and the 2D view of interaction profile of this ligand with surrounding amino acids of (a) PilF and (b) PilB.

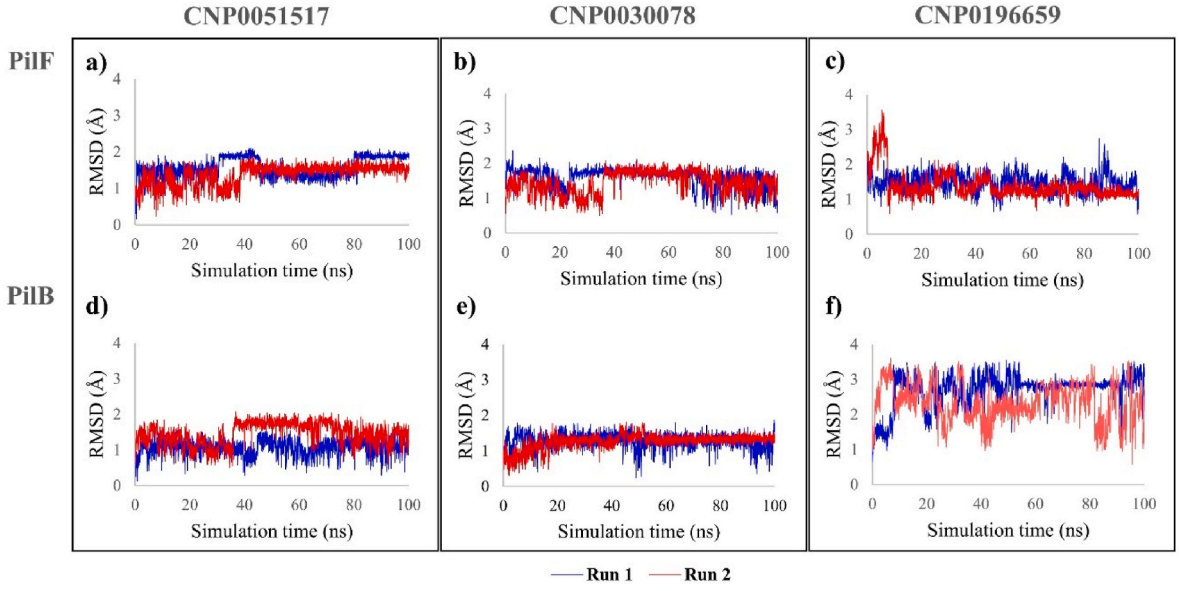

Fig. 5. Ligand RMSD profiles obtained from 2 parallel 100 ns MD simulations a) CNP0051517 bound to PilF, b) CNP0030078 bound to PilF, c) CNP00169659 bound to PilF, d) CNP0051517 bound to PilB, e) CNP0030078 bound to PilB, f) CNP00169659 bound to PilB complexes.

Furthermore, the distances measured between these valine residues and the selected ligands were all less than 3 Å indicating a strong interaction. We hypothesize that this residue has a critical role in the inhibition of T4 pili retraction since it (i) resides in the ADP binding region of the proteins, (ii) has a high occupancy rate among critical residues, and (iii) maintains the hydrophobic interaction with the ligands during the MD simulations. Thus, it should be considered to be among the target residues.

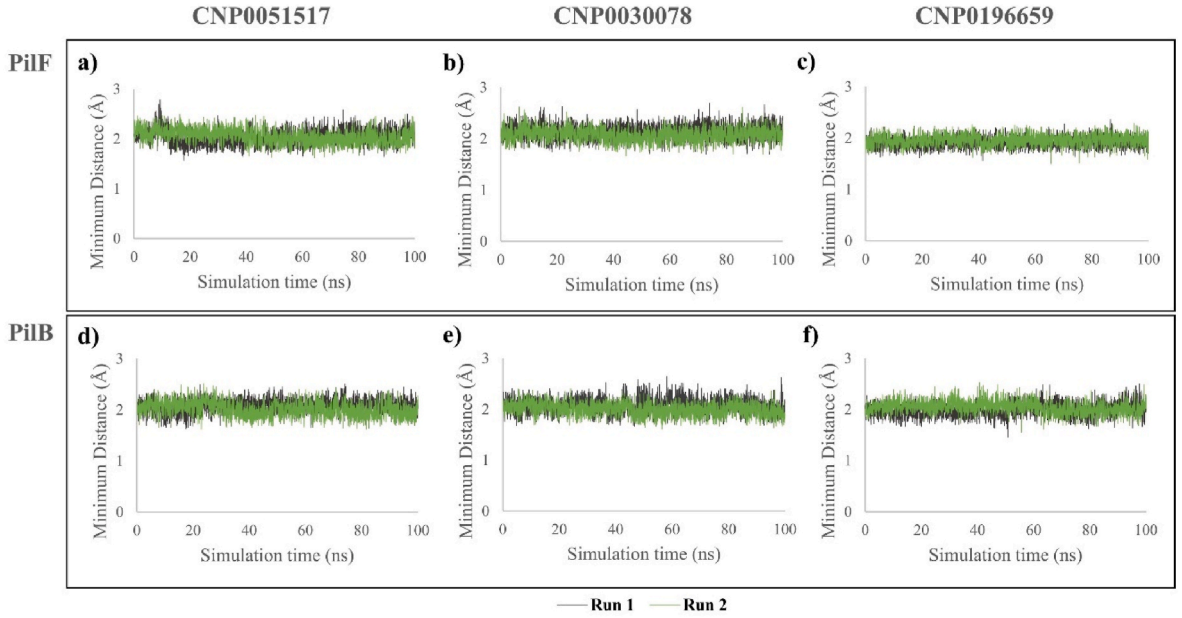

Fig. 6. The minimum distance between the proteins and ligands throughout the 100 ns MD simulations for 2 parallel runs. a) CNP0051517 bound to PilF, b) CNP0030078 bound to PilF, c) CNP00169659 bound to PilF, d) CNP0051517 bound to PilB, e) CNP0030078 bound to PilB, f) CNP00169659 bound to PilB complexes.

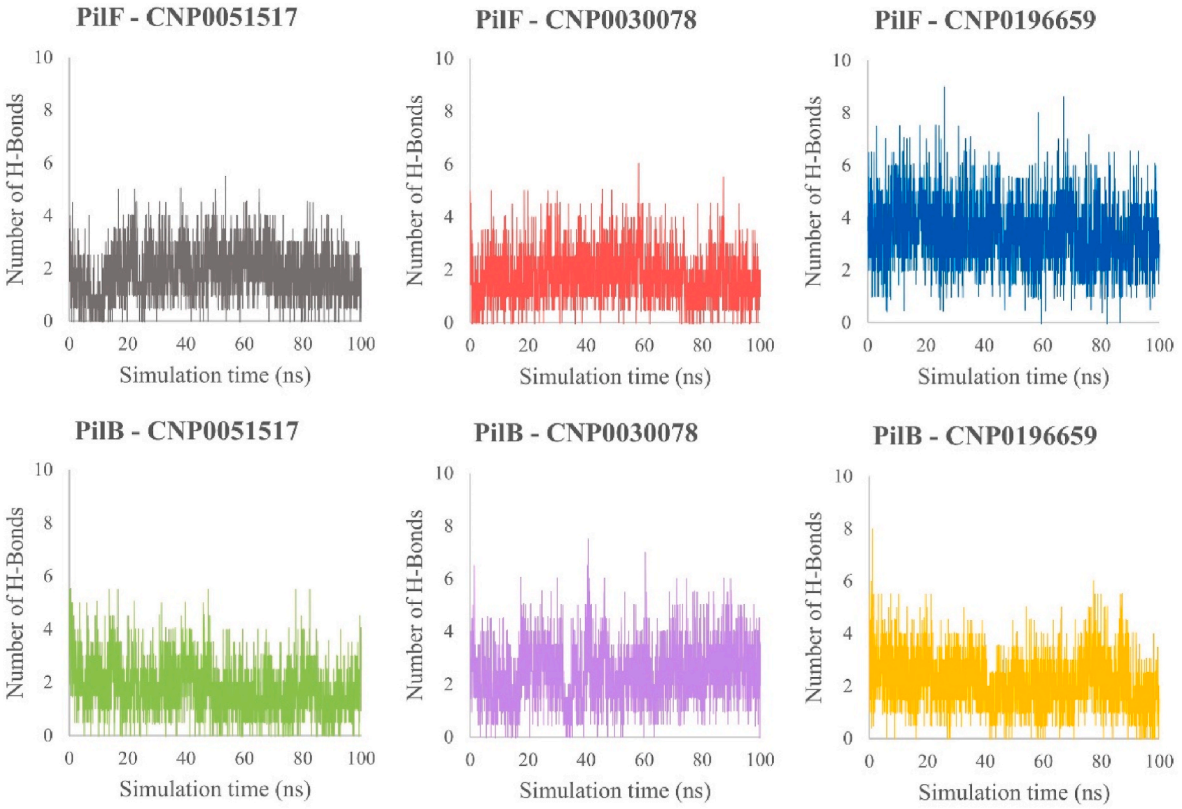

Fig. 7. Average number of H-bonds for 2 parallel 100 ns MD simulations between ligands (CNP001517, CNP0030078, and CNP0196659) and target proteins obtained from VMD.

MD simulations were further analyzed to investigate the stability of ligand binding. Available up-to-date literature [68–70] suggests that, around 100 ns of all-atom MD simulations provide important details about the molecular mechanism of protein–ligand interactions. The plots of ligand RMSD values obtained in this study from the simulations clearly showed that the selected ligands CNP0030078 and CNP0051517 remained stably bound to the target ATPases for 100 ns (especially from 40 ns onwards). On the other hand, CNP0196659 tented to be more flexible, especially in one of the simulations (Run 2 of CNP0196659 bound PilB). Upon careful examination during the 100 ns MD simulation

Table 3
Summary of average H-bond occupancy values among critical valine residues and the ligand molecules.

	Val323 of PilF	Val334 of PilB
CNP0051517	14.29%	23.87%
CNP0030078	16.47%	18.23%
CNP0196659	26.09%	17.69%

Table 4
Average binding free energies (MM/PBSA) of the potential ligands calculated for 50 snapshots retrieved from the last 20 ns of the 100 ns trajectories.

Ligand-protein complex	MM/PBSA (kcal/mol)
CNP0051517 bound to PilF	−13.61
CNP0030078 bound to PilF	−12.56
CNP00169659 bound to PilF	−9.66
CNP0051517 bound to PilB	−12.03
CNP0030078 bound to PilB	−12.80
CNP00169659 bound to PilB	−7.88

Table 5
Predicted bioactivities for CNP0051517, CNP0030078, and CNP0196659.

Ligand ID	Predicted Activity	Pa	Pi
CNP0051517	Analgesic. Non-opioid	0.692	0.012
	Cognition disorders treatment	0.668	0.008
	Dependence treatment	0.621	0.005
	Attention deficit	0.618	0.005
	Mood disorders treatment	0.622	0.014
	Antipsychotic	0.598	0.014
	Analgesic	0.603	0.026
	Antidepressant	0.542	0.020
	Antiparkinsonian	0.546	0.024
	Anti-obesity	0.546	0.027
	Sleep disorders treatment	0.521	0.005
	Anxiolytic	0.532	0.020
	Neurodegenerative diseases treatment	0.555	0.055
	Alzheimer's disease treatment	0.504	0.043
CNP0030078	Analgesic. Non-opioid	0.701	0.011
	Cognition disorders treatment	0.648	0.009
	Mood disorders treatment	0.627	0.013
	Antipsychotic	0.620	0.013
	Dependence treatment	0.612	0.005
	Analgesic	0.613	0.024
	Attention deficit	0.592	0.005
	Neurodegenerative diseases treatment	0.580	0.046
	Antidepressant	0.549	0.019
	Anxiolytic	0.545	0.019
	Anti-obesity	0.540	0.028
	Antiparkinsonian	0.536	0.026
	Sleep disorders treatment	0.512	0.005
	Alzheimer's disease treatment	0.530	0.035
CNP0196659	Gastrin inhibitor	0.600	0.023
	Spasmolytic, urinary	0.597	0.025
	CYP2A11 substrate	0.549	0.014
	Spasmolytic	0.539	0.022
	Spasmolytic, Papaverin-like	0.524	0.010
	Phosphatase inhibitor	0.521	0.094

trajectory, a slight flipping of the benzene ring of the ligand has been observed at some instances. This flipping enables greater flexibility in the tail region, hence affects the RMSD profile. Nevertheless, it still remained bound with a maximum of 4 Å in RMSD profiles and low H bonding distances (2.01 ± 0.13).

MM/PBSA calculation gives the total binding energy, which is a combination of electrostatic, van der Waals, SASA and polar solvation energy. Accordingly, lower binding energy indicates a higher binding affinity between the ligand and protein complex [71]. Based on this information, results obtained from free energy calculations supported the Autodock Vina binding affinity scores as CNP0051517 and CNP0030078 displayed lower free energy values than CNP00169659.

As a final step, special attention was paid on the biological activities of the candidate molecules to evaluate their potential. The activity profiles predicted by the PASS server displayed that CNP0051517 and CNP0030078 are more likely to be biologically active against nervous system-related diseases. There is also a recent study on the usage of drug compounds that contain piperidine against Alzheimer's disease, which is a nervous system-related disease. Using computational docking method together with *in vivo* and *in vitro* methods. Dias Viegas et al. [72] discovered new potential drugs effective against both neuroinflammation and neurodegenerative processes associated with Alzheimer's disease, all of which were multifunctional N-benzyl-piperidine-aryl-acylhydrazone derivatives containing piperidine. Their study certainly confirms the potential of piperidine containing drugs against nervous system-related diseases. Hence, piperidine containing CNP0051517 and CNP0030078 ligands' have potential to be used against *P. aeruginosa* and *N. meningitidis,* which are also known to cause central nervous system infections [8,18].

Moreover, CNP0051517 and CNP0030078 ligands share additional functional groups in addition to piperidine. Both ligands possess an aromatic ring with a benzoyl group, a trifluoromethyl group, and a phenyl group (Fig. S7). The benzoyl group is known to display antibacterial, comedolytic, and anti-inflammatory activities [73]. The trifluoromethyl group on the other hand is very important in medicinal chemistry to modulate physicochemical properties and increase drug molecule binding affinities [74]. The phenyl ring is found in the naturally occurring penicillin V structure. It is widely known that penicillin has historically been used for the treatment of laboratory-confirmed meningococcal infections [75]. On the other hand, among these functional groups the ligand CNP0196659 possessed only the benzoyl group. The topological polar surface area (TPSA) value of this ligand might be another reason why the ligand CNP0196659 is less promising than the other two ligands. This value is known as the surface sum over all polar atoms or molecules. It is a commonly used parameter for optimizing the ability of a drug to penetrate cells. Molecules with a TPSA greater than 140 $Å^2$ tend to be poor in penetrating cell membranes, while a TPSA of less than 90 $Å^2$ is usually required for molecules to penetrate the blood-brain barrier and thus act on receptors in the central nervous system [76,77]. Thus, we would expect the maximum TPSA value of the drug molecules to be 90 $Å^2$, since the microorganisms under question target the central nervous systems indirectly. While the TPSA values of the ligands CNP0051517 and CNP0030078 were 40.62 $Å^2$, the TPSA value of the ligand CNP0196659 was reported to be 82.14 $Å^2$ (*COCONUT: Natural Products Online*, 2022), a value very close to 90 $Å^2$. This also suggests why CNP0051517 and CNP0030078 ligands might be more potent than CNP0196659.

5. Conclusion

The docking-based virtual screening has identified piperidine-based inhibitors from the COCONUT natural products database against the elongation ATPases of T4 pili PilF and PilB of *N. meningitidis* and *P. aeruginosa*, respectively. The MD simulations further exhibited the stability of the bound structures. The predicted inhibitor binding pocket overlapped with the ATP/ADP binding site of the enzyme, which indicates that inhibitors may compete with ATP for binding. In particular, the hydrophobic interaction of a valine residue in the binding pockets of PilF and PilB structures with potential ligands provides clues regarding the possible inhibition mechanism of the ATPases. Among the top three binder molecules, those with COCONUT IDs CNP0030078 and CNP0051517 were predicted to possess biological activity against nervous system-related diseases, which suggests their potential in this antivirulence approach. Even, binding free energy estimations using the MM/PBSA method also reveal that CNP0051517 bound to PilF (−13.61 kcal/mol), CNP0030078 bound to PilF (−12.56 kcal/mol) and CNP0051517 bound to PilB (−12.03 kcal/mol) and CNP0030078 bound to PilB (−12.8 kcal/mol) are relatively more stable than CNP00169659

bound to PilF (−9.66 kcal/mol) and CNP00169659 bound to PilB (−7.88 kcal/mol). Further *in vivo* studies would help to confirm their activities. We believe that the findings of this work will serve as the basis for the discovery of new antivirulence chemotherapeutics possessing unique potential.

Author contributions

The manuscript was written through contributions of all authors. All authors have given approval to the final version of the manuscript.

Declaration of competing interest

The authors declare that they have no known competing financial interests or personal relationships that could have appeared to influence the work reported in this paper.

Data availability

Data will be made available on request.

Acknowledgment

Scientific and Technological Research Council of Turkey (TUBITAK) Project Number 120M225 is highly acknowledged. A.O. acknowledges YOK 100/2000.

Appendix A. Supplementary data

Supplementary data to this article can be found online at https://doi.org/10.1016/j.jmgm.2022.108382.

References

[1] B. Malik, S. Bhattacharyya, Antibiotic drug-resistance as a complex system driven by socio-economic growth and antibiotic misuse, Sci. Rep. 9 (2019) (2019) 1–12, https://doi.org/10.1038/s41598-019-46078-y, 91.
[2] A. Marra, Can virulence factors be viable antibacterial targets? Expert Rev. Anti Infect. Ther. 2 (2004) 61–72, https://doi.org/10.1586/14787210.2.1.61.
[3] C.L. Ventola, The antibiotic resistance crisis: part 1: causes and threats, P T 40 (2015) 277–283.
[4] T.L. Leighton, R.N.C. Buensuceso, P.L. Howell, L.L. Burrows, Biogenesis of Pseudomonas aeruginosa type IV pili and regulation of their function, Environ. Microbiol. 17 (2015) 4148–4163, https://doi.org/10.1111/1462-2920.12849.
[5] C.K. Ellison, T.N. Dalia, C.A. Klancher, J.W. Shaevitz, Z. Gitai, A.B. Dalia, Novel mechanisms of type IV pilus regulation in Acinetobacter baylyi, bioRxiv 2020 (2020), https://doi.org/10.1101/2020.09.28.317149, 09.28.317149.
[6] L. Craig, K.T. Forest, B. Maier, Type IV pili: dynamics, biophysics and functional consequences, Nat. Rev. Microbiol. 17 (2019) (2019) 429–440, https://doi.org/10.1038/s41579-019-0195-4, 177.
[7] R. Collins, V. Karuppiah, C.A. Siebert, R. Dajani, A. Thistlethwaite, J.P. Derrick, Structural cycle of the Thermus thermophilus PilF ATPase: the powering of type IVa pilus assembly, Sci. Rep. 8 (2018) 1–13, https://doi.org/10.1038/s41598-018-32218-3.
[8] J.E. Schmitz, C.W. Stratton, Neisseria meningitidis, in: Mol. Med. Microbiol, second ed., Elsevier Ltd, 2014, pp. 1729–1750, https://doi.org/10.1016/B978-0-12-397169-2.00098-6.
[9] S. Mühlen, P. Dersch, Anti-virulence strategies to target bacterial infections, Curr. Top. Microbiol. Immunol. 398 (2016) 147–183, https://doi.org/10.1007/82_2015_490.
[10] WHO, Meningococcal meningitis. https://www.who.int/news-room/fact-sheets/detail/meningococcal-meningitis, 2021. (Accessed 29 May 2021).
[11] C.-C. Ling, Bacterial polysaccharides: current innovations and future trends, in: Ullrich Matthias (Ed.), ChemBioChem, John Wiley & Sons, Ltd, 2009, pp. 2539–2540, https://doi.org/10.1002/CBIC.200900501.
[12] D.F. Blair, Pili and Flagella: Current Research and Future Trends, Horizon Scientific Press, Norfolk, UK, 2009.
[13] F. Wang, M. Coureuil, T. Osinski, A. Orlova, T. Altindal, G. Gesbert, X. Nassif, E. H. Egelman, L. Craig, Cryoelectron microscopy reconstructions of the Pseudomonas aeruginosa and Neisseria gonorrhoeae type IV pili at sub-nanometer resolution, Structure 25 (2017) 1423–1435, https://doi.org/10.1016/j.str.2017.07.016, e4.
[14] K. Denis, M. Le Bris, L. Le Guennec, J.P. Barnier, C. Faure, A. Gouge, H. Bouzinba-Ségard, A. Jamet, D. Euphrasie, B. Durel, N. Barois, P. Pelissier, P.C. Morand, M. Coureuil, F. Lafont, O. Join-Lambert, X. Nassif, S. Bourdoulous, Targeting Type IV pili as an antivirulence strategy against invasive meningococcal disease, Nat. Microbiol. 4 (2019) 972–984, https://doi.org/10.1038/s41564-019-0395-8.
[15] F. Aubey, J.P. Corre, Y. Kong, X. Xu, D. Obino, S. Goussard, C. Lapeyrere, J. Souphron, C. Couturier, S. Renard, G. Duménil, Inhibitors of the Neisseria meningitidis PilF ATPase provoke type IV pilus disassembly, Proc. Natl. Acad. Sci. U.S.A. 116 (2019) 8481–8486, https://doi.org/10.1073/pnas.1817757116.
[16] G. Duménil, Type IV pili as a therapeutic target, Trends Microbiol. 27 (2019) 658–661, https://doi.org/10.1016/j.tim.2019.05.005.
[17] D. Banerjee, D. Stableforth, The treatment of respiratory pseudomonas infection in cystic fibrosis: what drug and which way? Drugs 60 (2000) 1053–1064, https://doi.org/10.2165/00003495-200060050-00006.
[18] B.L. Wise, J.L. Mathis, E. Jawetz, Infections of the central nervous system due to pseudomonas aeruginosa, J. Neurosurg. 31 (1969) 432–434, https://doi.org/10.3171/jns.1969.31.4.0432.
[19] K. Kerr, A. Snelling, Pseudomonas aeruginosa: a formidable and ever-present adversary, J. Hosp. Infect. 73 (2009) 338–344.
[20] R.M. Donlan, J.W. Costerton, Biofilms : survival mechanisms of clinically relevant microorganisms, Clin. Microbiol. Rev. 15 (2002) 167–193, https://doi.org/10.1128/CMR.15.2.167.
[21] V.E. Wagner, L. Li, V.M. Isabella, B.H. Iglewski, Analysis of the hierarchy of quorum-sensing regulation in Pseudomonas aeruginosa, Anal. Bioanal. Chem. 387 (2007) 469–479, https://doi.org/10.1007/s00216-006-0964-6.
[22] D. Balasubramanian, L. Schneper, H. Kumari, K. Mathee, SURVEY AND SUMMARY A dynamic and intricate regulatory network determines Pseudomonas aeruginosa virulence, Nucleic Acids Res. 41 (2013) 1–20, https://doi.org/10.1093/nar/gks1039.
[23] K.J. Dye, N.J. Vogelaar, P. Sobrado, Z. Yang, High-throughput screen for inhibitors of the type IV pilus assembly ATPase PilB, mSphere 6 (2021), e00129, https://doi.org/10.1128/msphere.00129-21, 21.
[24] A. Waterhouse, M. Bertoni, S. Bienert, G. Studer, G. Tauriello, R. Gumienny, F. T. Heer, T.A.P. de Beer, C. Rempfer, L. Bordoli, R. Lepore, T. Schwede, SWISS-MODEL: homology modelling of protein structures and complexes, Nucleic Acids Res. 46 (2018) W296–W303.
[25] UniProt: the universal protein knowledgebase in 2021, Nucleic Acids Res. 49 (2021) D480–D489, https://doi.org/10.1093/nar/gkaa1100.
[26] V. Solanki, S. Kapoor, K.G. Thakur, Structural insights into the mechanism of Type IVa pilus extension and retraction ATPase motors, FEBS J. 285 (2018) 3402–3421, https://doi.org/10.1111/febs.14619.
[27] B. Huang, MetaPocket: A Meta Approach to Improve Protein Ligand Binding Site Prediction, vol. 13, 2009, pp. 325–330, https://doi.org/10.1089/OMI.2009.0045.
[28] A.C. Wallace, R.A. Laskowski, J.M. Thornton, LIGPLOT: a program to generate schematic diagrams of protein-ligand interactions, Protein Eng. 8 (1995) 127–134, https://doi.org/10.1093/PROTEIN/8.2.127.
[29] M. McCallum, S. Tammam, A. Khan, L.L. Burrows, P. Lynne Howell, The molecular mechanism of the type IVa pilus motors, Nat. Commun. 8 (2017) 1–10, https://doi.org/10.1038/ncomms15091.
[30] M. Sorokina, P. Merseburger, K. Rajan, M.A. Yirik, C. Steinbeck, COCONUT online: collection of open natural products database, J. Cheminf. 13 (2021) 1–13, https://doi.org/10.1186/S13321-020-00478-9.
[31] O. Jović, T. Šmuc, Search for novel lead inhibitors of yeast cytochrome bc1, from drugbank and COCONUT, Mol 26 (2021) 4323, https://doi.org/10.3390/MOLECULES26144323, 26 (2021) 4323.
[32] A.K. Sutliff, M. Saint-Cyr, A.E. Hendricks, S.S. Chen, K.A. Doenges, K. Quinn, J. Westcott, M. Tang, S.J. Borengasser, R.M. Reisdorph, W.W. Campbell, N. F. Krebs, N.A. Reisdorph, Lipidomics-based comparison of molecular compositions of green, yellow, and red bell peppers, Metabolites 11 (2021) 241, https://doi.org/10.3390/METABO11040241/S1.
[33] Y. Boulaamane, M.A.A. Ibrahim, M.R. Britel, A. Maurady, In silico studies of natural product-like caffeine derivatives as potential MAO-B inhibitors/AA2AR antagonists for the treatment of Parkinson's disease, J. Integr. Bioinform. (2022), 20210027, https://doi.org/10.1515/JIB-2021-0027, 0.
[34] F.D. Prieto-Martínez, E. Fernández-de Gortari, J.L. Medina-Franco, L. Michel Espinoza-Fonseca, An in silico pipeline for the discovery of multitarget ligands: a case study for epi-polypharmacology based on DNMT1/HDAC2 inhibition, Artif. Intell. Life Sci. 1 (2021), 100008, https://doi.org/10.1016/J.AILSCI.2021.100008.
[35] H. Hu, C. Hu, J. Peng, A.K. Ghosh, A. Khan, D. Sun, W. Luyten, Bioassay-guided interpretation of antimicrobial compounds in kumu, a TCM preparation from picrasma quassioides' stem via UHPLC-orbitrap-ion trap mass spectrometry combined with fragmentation and retention time calculation, Front. Pharmacol. 12 (2021) 2693, https://doi.org/10.3389/FPHAR.2021.761751.
[36] M.A. Miteva, S. Violas, M. Montes, D. Gomez, P. Tuffery, B.O. Villoutreix, FAF-Drugs: free ADME/tox filtering of compound collections, Nucleic Acids Res. 34 (2006), https://doi.org/10.1093/nar/gkl065.
[37] J.B. Baell, G.A. Holloway, New substructure filters for removal of pan assay interference compounds (PAINS) from screening libraries and for their exclusion in bioassays, J. Med. Chem. 53 (2010) 2719–2740, https://doi.org/10.1021/jm901137j.
[38] C.A. Lipinski, F. Lombardo, B.W. Dominy, P.J. Feeney, Experimental and computational approaches to estimate solubility and permeability in drug discovery and development settings, Adv. Drug Deliv. Rev. 64 (2012) 4–17, https://doi.org/10.1016/j.addr.2012.09.019.
[39] T.I. Oprea, Property distribution of drug-related chemical databases, J. Comput. Aided Mol. Des. 14 (2000) 251–264, https://doi.org/10.1023/A:1008130001697.
[40] J.J. Irwin, T. Sterling, M.M. Mysinger, E.S. Bolstad, R.G. Coleman, ZINC: a free tool to discover chemistry for biology, J. Chem. Inf. Model. 52 (2012) 1757–1768, https://doi.org/10.1021/ci3001277.

[41] C.A. Lipinski, Lead- and drug-like compounds: the rule-of-five revolution, Drug Discov. Today Technol. 1 (2004) 337–341, https://doi.org/10.1016/j.ddtec.2004.11.007.
[42] O. Trott, A.J. Olson, AutoDock Vina: improving the speed and accuracy of docking with a new scoring function, efficient optimization, and multithreading, J. Comput. Chem. 31 (2009), https://doi.org/10.1002/jcc.21334.
[43] D. S, O. AJ, Small-molecule library screening by docking with PyRx, Methods Mol. Biol. 1263 (2015) 243–250, https://doi.org/10.1007/978-1-4939-2269-7_19.
[44] BIOVIA Discovery Studio Visualizer, 2020.
[45] J.C. Phillips, D.J. Hardy, J.D.C. Maia, J.E. Stone, J.V. Ribeiro, R.C. Bernardi, R. Buch, G. Fiorin, J. Hénin, W. Jiang, R. McGreevy, M.C.R. Melo, B.K. Radak, R. D. Skeel, A. Singharoy, Y. Wang, B. Roux, A. Aksimentiev, Z. Luthey-Schulten, L. V. Kalé, K. Schulten, C. Chipot, E. Tajkhorshid, Scalable molecular dynamics on CPU and GPU architectures with NAMD, J. Chem. Phys. 153 (2020), 044130, https://doi.org/10.1063/5.0014475.
[46] J. Huang, S. Rauscher, G. Nawrocki, T. Ran, M. Feig, B.L. De Groot, H. Grubmüller, A.D. MacKerell, CHARMM36m: an improved force field for folded and intrinsically disordered proteins, Nat. Methods 14 (2016) 71–73, https://doi.org/10.1038/NMETH.4067.
[47] S. Kim, J. Lee, S. Jo, C.L. Brooks, H.S. Lee, W. Im, CHARMM-GUI ligand reader & modeler for CHARMM force field generation of small molecules, J. Comput. Chem. 38 (2017) 1879, https://doi.org/10.1002/JCC.24829.
[48] H. Liu, T. Hou, CaFE: a tool for binding affinity prediction using end-point free energy methods, Bioinformatics 32 (2016) 2216–2218, https://doi.org/10.1093/bioinformatics/btw215.
[49] L. Li, C. Li, S. Sarkar, J. Zhang, S. Witham, Z. Zhang, L. Wang, N. Smith, M. Petukh, E. Alexov, DelPhi: a comprehensive suite for DelPhi software and associated resources, BMC Biophys. 5 (2012) (2012) 1–11, https://doi.org/10.1186/2046-1682-5-9, 51.
[50] D.A. Filimonov, A.A. Lagunin, T.A. Gloriozova, A.V. Rudik, D.S. Druzhilovskii, P. V. Pogodin, V.V. Poroikov, Prediction of the biological activity spectra of organic compounds using the pass online web resource, Chem. Heterocycl. Compd. 50 (2014) 444–457, https://doi.org/10.1007/S10593-014-1496-1.
[51] S.K. Panigrahi, G.R. Desiraju, Strong and weak hydrogen bonds in the protein-ligand interface, Proteins Struct. Funct. Genet. 67 (2007) 128–141, https://doi.org/10.1002/PROT.21253.
[52] C.L. Giltner, Y. Nguyen, L.L. Burrows, Type IV pilin proteins: versatile molecular modules, Microbiol. Mol. Biol. Rev. 76 (2012) 740–772, https://doi.org/10.1128/MMBR.00035-12.
[53] L.L. Burrows, Pseudomonas aeruginosa Twitching Motility: Type IV Pili in Action, vol. 66, 2012, pp. 493–520, https://doi.org/10.1146/annurev-micro-092611-150055.
[54] M. Sorokina, C. Steinbeck, Review on natural products databases: where to find data in 2020, J. Cheminf. 12 (2020) 1–51, https://doi.org/10.1186/s13321-020-00424-9.
[55] N. Leeantha, K.N. Venugopala, S. Francis, O. Bharti, Antimicrobial and antioxidant activities of piperidine derivatives, African J. Pharm. Pharmacol. 9 (2015) 783–792, https://doi.org/10.5897/ajpp2015.4335.
[56] G.N. Ramachandran, Protein structure and crystallography, Science (80-) 141 (1963) 288–291.
[57] R.A. Laskowski, M.W. MacArthur, D.S. Moss, J.M. Thornton, IUCr, PROCHECK: a program to check the stereochemical quality of protein structures, J. Appl. Crystallogr. 26 (1993) 283–291, https://doi.org/10.1107/S0021889892009944.
[58] D. Eisenberg, R. Lüthy, J.U. Bowie, VERIFY3D: assessment of protein models with three-dimensional profiles, Methods Enzymol. 277 (1997) 396–404, https://doi.org/10.1016/S0076-6879(97)77022-8.
[59] C. Colovos, T.O. Yeates, Verification of protein structures: patterns of nonbonded atomic interactions, Protein Sci. 2 (1993) 1511–1519, https://doi.org/10.1002/pro.5560020916.
[60] J. Elkaim, M. Castroviejo, D. Bennani, S. Taouji, N. Allain, M. Laguerre, J. Rosenbaum, J. Dessolin, P. Lestienne, First identification of small-molecule inhibitors of Pontin by combining virtual screening and enzymatic assay, Biochem. J. 443 (2012) 549–559, https://doi.org/10.1042/BJ20111779.
[61] G. Zhang, S. Li, K.W. Cheng, T.F. Chou, AAA ATPases as therapeutic targets: structure, functions, and small-molecule inhibitors, Eur. J. Med. Chem. 219 (2021), 113446, https://doi.org/10.1016/J.EJMECH.2021.113446.
[62] K.J. Dye, Z. Yang, Cyclic-di-GMP and ADP bind to separate domains of PilB as mutual allosteric effectors, Biochem. J. 477 (2020) 213–226, https://doi.org/10.1042/BCJ20190809.
[63] C. Bissantz, B. Kuhn, M. Stahl, A medicinal chemist's guide to molecular interactions, J. Med. Chem. 53 (2010) 5061–5084, https://doi.org/10.1021/jm100112j.
[64] S.V. Kathuria, Y.H. Chan, R.P. Nobrega, A. Özen, C.R. Matthews, Clusters of isoleucine, leucine, and valine side chains define cores of stability in high-energy states of globular proteins: sequence determinants of structure and stability, Protein Sci. 25 (2016) 662, https://doi.org/10.1002/PRO.2860.
[65] J.S. Chauhan, N.K. Mishra, G.P.S. Raghava, Identification of ATP binding residues of a protein from its primary sequence, BMC Bioinf. 10 (2009) 434, https://doi.org/10.1186/1471-2105-10-434.
[66] A.M. Hockenberry, D.M. Hutchens, A. Agellon, M. So, Attenuation of the type IV pilus retraction motor influences Neisseria gonorrhoeae social and infection behavior, mBio 7 (2016), https://doi.org/10.1128/MBIO.01994-16.
[67] F. Guerra, M. Siemers, C. Mielack, A.-N. Bondar, Dynamics of long-distance hydrogen-bond networks in photosystem II, J. Phys. Chem. B 122 (2018) 4, https://doi.org/10.1021/acs.jpcb.8b00649.
[68] M.T. Khan, A. Ali, Q. Wang, M. Irfan, A. Khan, M.T. Zeb, Y.J. Zhang, S. Chinnasamy, D.Q. Wei, Marine natural compounds as potents inhibitors against the main protease of SARS-CoV-2-a molecular dynamic study, J. Biomol. Struct. Dyn. (2020), https://doi.org/10.1080/07391102.2020.1769733.
[69] H. Guterres, W. Im, Improving protein-ligand docking results with high-throughput molecular dynamics simulations, J. Chem. Inf. Model. 60 (2020) 2189–2198, https://doi.org/10.1021/acs.jcim.0c00057.
[70] B. Ahmad, M. Batool, Q.U. Ain, M.S. Kim, S. Choi, Exploring the binding mechanism of PF-07321332 SARS-CoV-2 protease inhibitor through molecular dynamics and binding free energy simulations, Int. J. Mol. Sci. 22 (2021), https://doi.org/10.3390/ijms22179124.
[71] A.D. Elmezayen, Y. Kemal, Structure-based virtual screening for novel potential selective inhibitors of class IIa histone deacetylases for cancer treatment, Comput, Biol. Chem. 92 (2021), 107491, https://doi.org/10.1016/J.COMPBIOLCHEM.2021.107491.
[72] F.P. Dias Viegas, M. de Freitas Silva, M. Divino da Rocha, M.R. Castelli, M. M. Riquiel, R.P. Machado, S.M. Vaz, L.M. Simões de Lima, K.C. Mancini, P. C. Marques de Oliveira, É.P. Morais, V.S. Gontijo, F.M.R. da Silva, D. D'Alincourt da Fonseca Peçanha, N.G. Castro, G.A. Neves, A. Giusti-Paiva, F.C. Vilela, L. Orlandi, I. Camps, M.P. Veloso, L.F. Leomil Coelho, M. Ionta, G.Á. Ferreira-Silva, R.M. Pereira, L.E. Dardenne, I.A. Guedes, W. de Oliveira Carneiro Junior, P. M. Quaglio Bellozi, A.C. Pinheiro de Oliveira, F.F. Ferreira, L. Pruccoli, A. Tarozzi, C. Viegas, Design, synthesis and pharmacological evaluation of N-benzyl-piperidinyl-aryl-acylhydrazone derivatives as donepezil hybrids: discovery of novel multi-target anti-alzheimer prototype drug candidates, Eur. J. Med. Chem. 147 (2018) 48–65, https://doi.org/10.1016/J.EJMECH.2018.01.066.
[73] National Center for Biotechnology Information, PubChem compound summary for CID 19766641, CID 19766641. https://pubchem.ncbi.nlm.nih.gov/compound/19766641, 2022. (Accessed 1 June 2022).
[74] D. Kumar, V. Arun, M. Pilania, N.M. Kumar, Organohypervalent iodine reagents in the synthesis of bioactive heterocycles, in: Green Synth. Approaches Biol. Relev. Heterocycles, Elsevier Inc., 2014, pp. 353–379, https://doi.org/10.1016/B978-0-12-800070-0.00014-1.
[75] X.Y. Sun, M.Y. Liu, C.Y. Zhong, G.L. Zheng, M.Y. Lv, B.T. Jing, C.Y. Pan, X. Wang, Synthesis and antibacterial evaluation of 2-ethyl-1-(4-substituted)phenyl- 1h-imidazole derivatives as open-chain analogues of 7-Alkoxyl-4,5-dihydro-imidazo [1,2-A]quinolines, J. Braz. Chem. Soc. 29 (2018) 701–707, https://doi.org/10.21577/0103-5053.20170190.
[76] H. Pajouhesh, G.R. Lenz, Medicinal chemical properties of successful central nervous system drugs, NeuroRx 2 (2005) 541–553, https://doi.org/10.1602/NEURORX.2.4.541.
[77] S.A. Hitchcock, L.D. Pennington, Structure-brain exposure relationships, J. Med. Chem. 49 (2006) 7559–7583, https://doi.org/10.1021/JM060642I.